Ridge Waveguides and Y-Branch Beam Splitters in KTiOAsO4 Crystal by 15 MeV Oxygen Ion Implantation and Femtosecond Laser Ablation

Chen, C.; Akhmadaliev, S.; Romero, C.; de Aldana, J.; Zhou, S.; Chen, F.;

Ridge waveguides and Y-branch beam splitters in KTiOAsO$_4$ crystal by 15 MeV oxygen ion implantation and femtosecond laser ablation

Chen Chen, Shavkat Akhmadaliev, Carolina Romero, Javier R. Vázquez de Aldana, Shengqiang Zhou, and Feng Chen, *Senior Member, OSA*

Abstract—**We report on the fabrication of ridge waveguides and Y-branch beam splitters in KTiOAsO$_4$ (KTA) nonlinear optical crystal by the combination of 15 MeV oxygen (O^{5+}) ion implantation and femtosecond laser ablation. Guiding properties were investigated at the wavelengths of 633 and 808 nm, respectively, showing high polarization sensitivity of light propagation. Splitting ratios of these beam splitters are dependent on in-coupling alignment. The simulated guiding modal distributions of splitted guided beams, which was based on a reconstructed refractive index profile, shows reasonable consistence with the measured ones. After the stepwise annealing treatment at 473 and 573 K for 1 hour each, the propagation losses for these guiding structures have been reduced considerably.**

Index Terms—**Potassium titanyle arsenate, Ridge waveguides, Beam splitters, Ion implantation, Laser ablation.**

I. INTRODUCTION

As an excellent nonlinear optical crystal, potassium titanyl arsenate (KTiOAsO$_4$ or KTA) possesses large nonlinear optical and electro-optical coefficients, as well as high damage threshold. In comparison to the more well-known potassium titanyl phosphate (KTiOPO$_4$ or KTP) crystal, the KTA has the additional advantage of reduced absorption at the wavelength of 2 to 5 µm range [1,2]. In addition, a number of attractive nonlinear optical applications involving KTA crystal have been realized for second harmonic generation (SHG), sum and difference frequency generation (SFG and DFG), optical parametric oscillation/amplification (OPO/OPA), and electro-optical switching involving mid-infrared (MIR) wavelengths [3-6].

C. Chen and F. Chen are with the School of Physics, State Key Laboratory of Crystal Materials, Shandong University, Jinan 250100, China (e-mail: chchgogogo@163.com; drfchen@sdu.edu.cn).
S. Akhmadaliev and S. Zhou are with Helmholtz-Zentrum Dresden-Rossendorf, Institute of Ion Beam Physics and Materials Research, Dresden 01328, Germany (e-mail: c.akhmadaliev@hzdr.de; s.zhou@hzdr.de).
C. Romero and J. R. Vázquez de Aldana are with the Laser Microprocessing Group, Universidad de Salamanca, Salamanca 37008, Spain (e-mail: cromero@usal.es; jrval@usal.es).

Integrated photonics enables various on-chip functions through the platforms of compact and diffraction-free waveguide-based photonic systems. Optical waveguide, as one of the basic elements in integrated photonics, is able to localize light propagation within the volume of micron scale, and consequently enhance the intracavity light intensity compared with that in the bulks [7,8]. In addition, the Y-branch waveguide is an important passive device in optical integrated circuits that can be used as beam splitters, optical switches, phase modulators and biosensors [9-15]. Recently, it has been reported that, by applying Y-branched geometries, efficient lasing or frequency doubling (through SHG) can be implemented by direct optical pump [16-19], which offers new applications for the Y-branch waveguides in laser or nonlinear crystals.

The first significant step to realize Y-branches is to fabricate waveguides in optical materials. A number of approaches, such as ion exchange/in-diffusion, thin film deposition, ion implantation/irradiation, and ultrafast laser inscription, have been introduced so far for waveguide fabrications in numerous optical materials [20-23]. Ion implantation/irradiation has been universally utilized for waveguide productions owing to its flexible modification of refractive index at certain depth by adjusting ion species, energy and fluence [24,25]. In order to build two-dimensionally (2D) confined waveguides (channel, ridge, etc.) and more complicated structures (Y-branch splitter, directional coupler, etc.), surface patterning technologies are necessary to be incorporated. Such technologies contain lithography, chemical etching, diamond blade dicing and laser ablation [26-28]. Ultrafast laser ablation has been proven to be a feasible and simple method to manufacture ridged guiding structures in several optical materials, including single crystals and glasses [29-32].

In this work, we report on the production of ridge waveguides and Y-branch beam splitters on a KTA sample through 15 MeV O^{5+} ion implantation followed with femtosecond laser ablation. Owing to the KTA bulk features, the high-quality waveguides and beam splitters based on KTA crystal platform could be used for realization of on-chip nonlinear frequency conversion and electro-optical switching/modulation, which have potential applications in the areas of integrated photonics and nonlinear optics. In this work, the guiding properties of the KTA ridge structures have been

investigated experimentally, which are in good agreement with the simulation.

II. EXPERIMENTAL IN DETAILS

The KTA sample used in this work was grown by the Czochralski technique (provided by Crystech Inc., China), and cut into a wafer with the dimension of 10 (x)×8 (y)×1 (z) mm^3 (x, y, z represents the dielectric axis of KTA crystal), of which two end faces 8×1 mm^2 and a top surface 10×8 mm^2 were optically polished. Figures 1(a) and (b) show the schematic plots of the ridge and Y-branch waveguide fabrication. In the first step, the sample was implanted by 15 MeV O^{5+} ions at the fluence of 4×10^{14} ions/cm^2, carried out through a 3MV tandem accelerator at Helmholtz-Zentrum Dresden-Rossendorf, Germany. The incident angle of the ion beam was determined to be 7° (i.e., the beam was titled by 7° off the normal plane of 10×8 mm^2) in order to avoid the channeling effect. Meanwhile, the ion beam current density was kept less than 10 nA/cm^2 to prevent the sample from charging and heating. After the implantation, a planar layer with refractive index modification (i.e., planar waveguide layer) was formed on top of the sample surface.
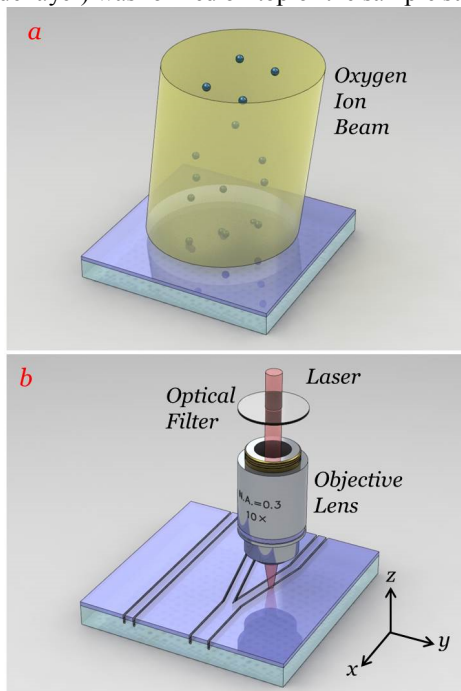

Fig. 1. The schematic diagrams of waveguides fabrication processes: (a) 15 MeV O^{5+} ion implantation, (b) femtosecond laser ablation.

Afterwards, the top surface of the sample (i.e., planar waveguide layer) was patterned by a Ti:Sapphire femtosecond laser system with a linearly polarized light (parallel with the y dielectric axis of KTA crystal) at 796 nm (with a pulse duration of 120 fs, and a repletion rate of 1 kHz). The laser beam, focused through a microscope objective lens (10×, N.A. = 0.3), scanned the sample which was mounted on a 3-axis motorized stage. The scan velocity and pulse energy were decided to be 50 μm/s and 0.7 μJ, respectively, for optimization after several tests for different parameters. A number of pairs of laser ablated air grooves (deeper than the ion implanted layer, as cross

sectional microscopic photograph shown in Fig. 2(a)) were produced on sample surface, separating the region into many stripe ridges, including ridge waveguide and Y-branch waveguide beam splitters. Please note that the air groves served as refractive index wells for the horizontal confinement of guided light. The widths of the ridges were defined to be 20-100μm, respectively. The roughness of the sidewalls of the air grooves was ~1μm, which was in good agreement with that reported in literatures on femtosecond laser ablated dielectrics [30-32].

The optical guiding properties of these two beam splitters were investigated by employing a typical end-face coupling arrangement [30]. The arrangement consisted of two microscope objectives (as coupling lenses), a half-wave plate (as the linear polarizer), a CCD camera and a powermeter. The light source was either a He-Ne laser of 633 nm wavelength or a Ti:Sapphire laser operated at 808 nm. In addition, in order to study the ion implantation induced effects on the microcosmic structure of KTA crystal, we measured micro-Raman emission spectra from different positions (substrate and implanted layer), with the excitation of blue light at wavelength of 473 nm. The scattering signals were collected and analyzed by a confocal microscope/spectrometer (Horiba/Jobin Yvon HR800).

The propagation losses were estimated for different guiding structures by directly measuring the input and output light powers though the waveguides. For the calculation of the loss coefficients, we have taken into account the Fresnel reflections and coupling efficiencies from focused light beam to the waveguides, which could be obtained from the respective overlap integrals.

III. RESULTS AND DISCUSSION

Figure 2(b) and (c) illustrate the TE guided modes (polarization parallel with dielectric axis y) at 633 and 808 nm in the 25μm wide KTA ridge waveguide and the output powers as a function of polarized direction for input light at 633 nm drawn in a polar coordinate system. One can find that the waveguiding effect is sensitive to the polarization of light. When the light is polarized alone TE direction (i.e., 0° and 180°), the strongest power is obtained, whilst the weakest power along TM polarization (i.e., 90° and 270°) remains only around 10% of the maximum value. This phenomenon is also found in other guiding structures and is related to the anisotropic refractive index of KTA crystal. As a consequence, the confinement abilities differ for the light in different polarization.

The microscopic photographs of the KTA Y-branch beam splitters taken from top surface are depicted in Figure 3. The beam splitter No. 1 has the width of 60 and 30 μm for the input and output arm each, with a splitting angle of 1.5°. While for beam splitter No. 2, the width for the input and output arm is 80 and 40 μm each, splitting by the angle of 2°. The guiding modal distributions of these beam splitters are also presented in Figure 3, for TE modes at 633 and 808 nm respectively. Splitting ratios of these splitters are dependent on the in-coupling alignment, and splitting ratio of 1:1 could be realized if the light spot was aligned on the middle position of the input area. It should be

noted that the guided modes are single (TE_{00}) in 25, 35 µm-wide waveguides at both 633 and 808 nm, in 60/30, 80/40 µm-wide splitters at 808 nm, and laterally multiple ($TE_{10,20}$) for other cases.
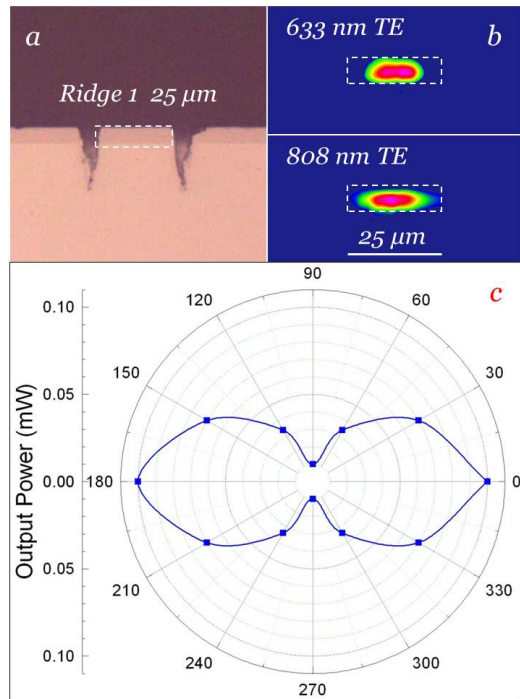

Fig. 2. The microscopic photograph at the cross section (a), the measured TE modal distributions at the wavelength of 633 and 808 nm (b) and the output powers versus light polarization angle (c) for 25 µm-wide KTA ridge waveguide.
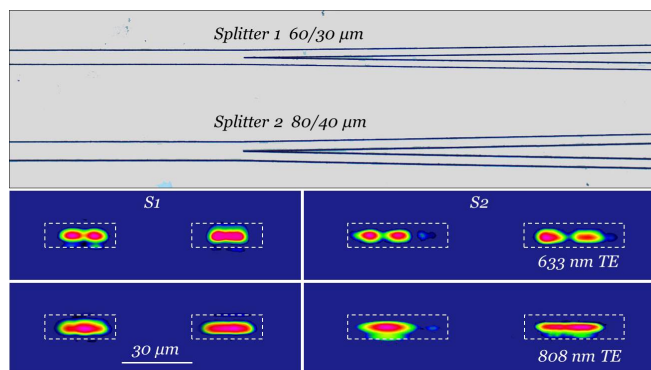

Fig. 3. The microscopic photograph at the top surface (top) and the measured TE modal distributions at 633 and 808 nm (bottom) for KTA y-branch beam splitters.

The interactions between incident O^{5+} ions and the target KTA crystal during implantation was simulated by using the code of Stopping and Range of Ions in Matter 2013 (SRIM 2013) [33], which is on the basis of Monte Carlo approach. The energy deposition of incident O^{5+} ions onto the KTA crystal is mainly through two mechanisms: electronic excitation (related to electronic stopping power S_e) and nuclear collision (related to nuclear stopping power S_n). From Figure 4(a) we find that the calculated S_e and S_n of O^{5+} ions have different variations against penetration depth. The S_e stays at a relatively high level (>2.0 keV/nm) from surface to the peak position at the depth of ~4.5 µm. The S_n remains unnoticeable from surface to the depth of

~6 µm, and grows rapidly to a maximum value of ~0.25 keV/nm at ~7.8 µm. The stopping powers start to be absent at the end of ion projected range (~8.2 µm), which agrees with the thickness of waveguide layer (Figure 2(a)).
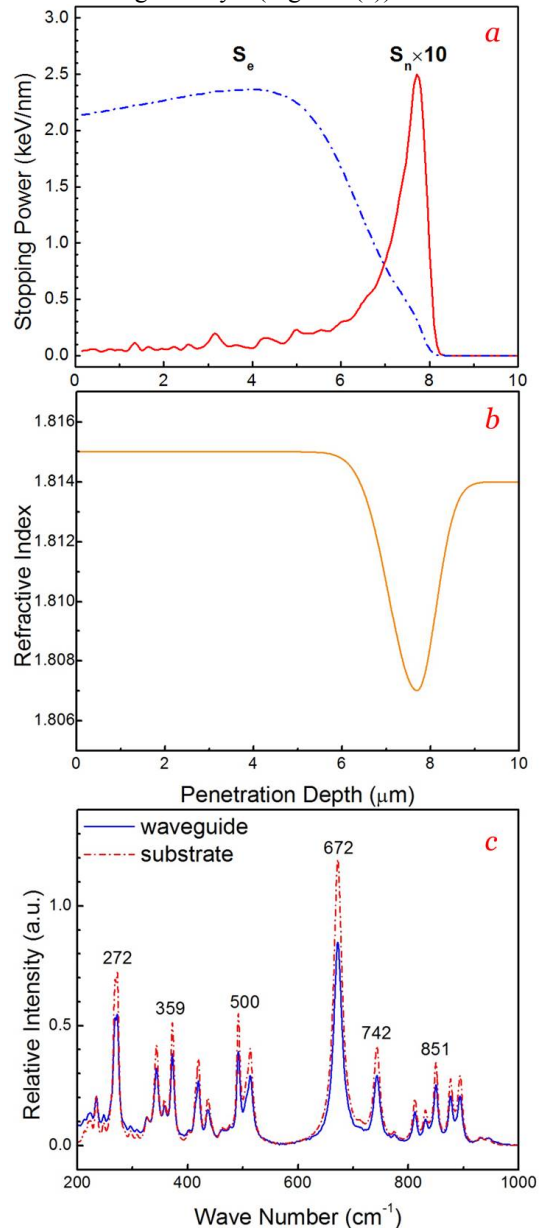

Fig. 4. (a) The electronic (S_e) and nuclear (S_n) stopping powers versus penetration depth beneath the surface for oxygen ions into KTA sample; (b) the reconstructed refractive index profile of the waveguide region; (c) the micro Raman spectra from the implanted and substrate region of KTA sample.

Figure 4(c) presents the micro-Raman emission spectra collected from substrate and the implanted layer of KTA sample. The spectra contain several peaks that are located respectively at the wave numbers of 272, 359, 500, 672, 742 and 851 cm^{-1}. The intensities from the implanted region at peak positions are about 30% lower in comparison to the bulk, suggesting that the energetic O^{5+} ions have induced certain lattice damage and disorder inside the implanted region. On the other hand, high similarity is observed in such two spectra without significant shift of the peak positions, indicating that

the basic structure and optical properties could be preserved after the implantation process.

Figure 4(b) displays the reconstructed refractive index profile of KTA sample for TE mode (n_y) at 633 nm. The displacement damage of lattice atoms due to nuclear energy loss contributes to a decrease of refractive index at the end of ions trajectory, which is commonly known as an optical barrier. The partial disorder of lattice correlated with electronic energy loss contributes to a slight increase in the near surface region. The maximum contrast of the refractive index Δn (~0.008) was given by the following equation:

$$\Delta n = \frac{\sin^2 \Theta_m}{2n} \qquad (1)$$

where n (1.814) is the substrate refractive index of the sample, and Θ_m the maximum incident angle (9.8°), which is the largest angle allowed between the incident light beam and the sample end-face normal.

Depending on the index distribution, the simulation of light propagation within beam splitting splitter 1 was operated using a software Rsoft Beam PROP 8.0 [34], which is based upon the finite difference beam propagation method (FD-BPM) [35].
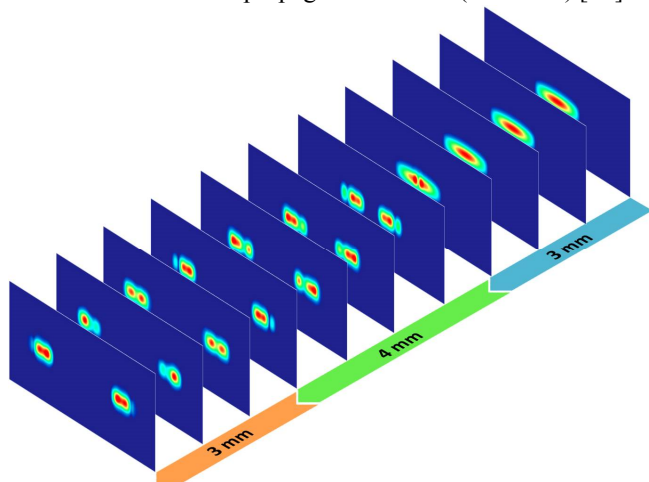

Fig. 5. The simulated modal distributions at the wavelength of 633 nm for beam splitter No. 1 at different locations along the propagation path.

Figure 5 gives the evolutions of guided mode at different locations (every 1 mm from 0 to 10 mm along x axis). The simulated output mode agrees quite well with the experimental result (as shown in Figure 2(b)), indicating that the reconstructed index profile is reasonable to reflect the real case.

TABLE I
THE PROPAGATION LOSSES OF RIDGE WAVEGUIDES AND BEAM SPLITTERS FOR TE MODES AT 633 NM

Waveguide Configuration	Width (μm)	Propagation Loss (dB/cm)		
		No Treatment	473 K for 1h	573 K for 1h
Ridge	45	2.8	2.1	1.7
	35	3.2	2.7	2.4
	25	3.5	2.9	2.8
Y-branch	80/40	4.9	4.1	3.6
	60/30	5.2	4.4	3.9

Table 1 lists the propagation losses of ridge waveguides and beam splitters for TE modes at 633 nm. It can be found that as the loss value of ridge decreases with the width. Loss in beam splitter is relatively higher possibly due to the addition loss in the bending parts and splitting junction. After stepwise annealing treatments in a tubular oven at 473 and 573 K for 1 h each, the losses have been reduced obviously, since some point defects and color centers (i.e. absorption site) induced by ion implantation have been gradually modified.

IV. CONCLUSION

Y-Branch beam splitters and ridge waveguides were manufactured in KTA nonlinear crystal by O^{5+} ion implantation along with femtosecond laser ablation. The guiding properties investigated at the wavelength of 633 and 808 nm shows high polarization sensitivity of these guiding structures, with the splitting ratios dependent on in-coupling alignment. The simulated guiding mode for beam splitter No. 1, depending on a reconstructed index profile, has great consistence with the measured one. Through stepwise annealing treatment at 473 and 573 K for 1 hour each, the propagation losses of guiding structures could be reduced significantly.

REFERENCES

[1] Z. L. Gao, Y. X. Sun, X. Yin, S. P. Wang, M. H. Jiang, and X. T. Tao, "Growth and electric-elastic properties of KTiOAsO$_4$ single crystal," *J. Appl. Phys.*, vol. 108, no. 2, pp. 024103, Jul. 2010.
[2] D. N. Nikogosyan, Nonlinear optical crystals: a complete survey. New York: Springer, 2005.
[3] P. Zeil, A. Zukauskas, S. Tjornhammar, C. Canalias, V. Pasiskevicius, and F. Laurell, "High-power continuous-wave frequency-doubling in KTiOAsO$_4$," *Opt. Express*, vol. 21, no. 25, pp. 30453-30459, Dec. 2013.
[4] Y. Baravets, P. Honzatko, F. Todorov, and P. Gladkov, "Narrowband widely tunable CW mid-infrared generator based on difference frequency generation in periodically poled KTP and KTA crystals," *Opt. Quant. Electron.*, vol. 48, no. 5, pp. 286, May 2016.
[5] M. S. Webb, P. F. Moulton, J. J. Kasinski, R. L. Burnham, G. Loiacono, and R. Stolzenberger, "High-average-power KTiOAsO$_4$ optical parametric oscillator," *Opt. Lett.*, vol. 23, no. 15, pp. 1161-1163, Aug. 1998.
[6] K. Zhong, Y. Y. Wang, D. G. Xu, Y. F. Geng, J. L. Wang, P. Wang, and J. Q. Yao, "Efficient electro-optic Q-switched eye-safe optical parametric oscillator based on KTiOAsO$_4$," *Appl. Phys. B*, vol. 97, no. 1, pp. 61-66, Sep. 2009.
[7] G. Lifante, Integrated Photonics: Fundamentals. Atrium: Wiley, 2008.
[8] E. J. Murphy, Integrated optical circuits and components: Design and applications. New York: Marcel Dekker, 1999.
[9] T. Hu, H. D. Qiu, Z. C. Zhang, X. Guo, C. Y. Liu, M. S. Rouifed, C. G. Littlejohns, G. T. Reed, and H. Wang, "A Compact Ultrabroadband Polarization Beam Splitter Utilizing a Hybrid Plasmonic Y-Branch," *IEEE Photonics J.*, vol. 8, no. 4, Aug. 2016.
[10] X. G. Tang, J. K. Liao, H. P. Li, and Y. Z. Liu, "Novel Approach for Controllable Polarization Beam Splitter: Design and Simulation," *IEEE J. Quantum Electron.*, vol. 49, no. 1, pp. 43-50, Jan. 2013.
[11] T. Chantakit, K. Srinuanjan, and P. P. Yupapin, "Two dimension photonic crystal Y-branch beam splitter with variation of splitting ratio based on hybrid defect controlled," *Appl. Phys. A*, vol. 117, no. 2, pp. 547-552, Nov. 2014.
[12] M. N. Khan, J. E. Zucker, T. Y. Chang, N. J. Sauer, M. D. Divino, T. L. Koch, C. A. Burrus, and H. M. Presby, "Design and demonstration of weighted-coupling digital Y-branch optical switches in InGaAs/InGaAlAs electron transfer waveguides," *J. Lightwave Technol.*, vol. 12, no. 11, pp. 2032-2039, 1994.
[13] J. H. Kim and H. H. Park, "Total internal reflection optical switch using the reverse breakdown of a pn junction in silicon," *Opt. Lett.*, vol. 40, no. 21, pp. 4859-4862, Nov. 2015.

[14] G. T. Paloczi, Y. Huang, A. Yariv, J. Luo, and A. K. Y. Jen, "Replica-molded electro-optic polymer Mach-Zehnder modulator," *Appl. Phys. Lett.*, vol. 85, no. 10, pp. 1662-1664, Sep. 2004

[15] A. H. Reshak, M. M. Shahimin, K. N. Khor, M. H. A. Wahid, and N. Hambali, "Evanescent field optimization on Y-branch silicon nitride optical waveguide for biosensing," *Mater. Lett.*, vol. 173, pp. 127-130, Jun. 2016.

[16] H. L. Liu, J. R. V. de Aldana, M. H. Hong, and F. Chen, "Femtosecond Laser Inscribed Y-Branch Waveguide in Nd:YAG Crystal: Fabrication and Continuous-Wave Lasing," *IEEE J. Sel. Top. Quant. Electron.*, vol. 22, no. 2, pp. 1-4, Apr. 2016.

[17] H. L. Liu, C. Cheng, C. Romero, J. R. Vazquez de Aldana, and F. Chen, "Graphene-based Y-branch laser in femtosecond laser written Nd:YAG waveguides," *Opt. Express*, vol. 23, no. 8, pp. 9730-9735, Apr. 2015.

[18] T. Calmano, C. Krankel, and G. Huber, "Laser oscillation in Yb:YAG waveguide beam splitter with variable splitting ratio," *Opt. Lett.*, vol. 40, no. 8, pp. 1753–1756, Apr. 2015.

[19] W. Nie, Y. Jia, J. R. Vázquez de Aldana, and F. Chen, "Efficient Second Harmonic Generation in 3D Nonlinear Optical-Lattice-Like Cladding Waveguide Splitters by Femtosecond Laser Inscription," *Sci. Rep.-UK*, vol. 6, pp. 22310, Feb. 2016.

[20] M. A. Butt, M. C. Pujol, R. Sole, A. Rodenas, G. Lifante, J. S. Wilkinson, M. Aguilo, and F. Diaz, "Channel waveguides and Mach-Zehnder structures on RbTiOPO$_4$ by Cs$^+$ ion exchange," *Opt. Mater. Express*, vol. 5, no. 5, pp. 1183-1194, May. 2015.

[21] G. Ulliac, V. Calero, A. Ndao, F. I. Baida, and M. P. Bernal, "Argon plasma inductively coupled plasma reactive ion etching study for smooth sidewall thin film lithium niobate waveguide application," *Opt. Mater.*, vol. 53, pp. 1-5, Mar. 2016.

[22] Y. Jiang, K. M. Wang, X. L. Wang, C. L. Jia, L. Wang, Y. Jiao, Q. M. Lu, H. J. Ma, R. Nie, and D. Y. Shen, "Planar optical waveguide in potassium titanyl arsenate formed by oxygen ion implantation at low doses," *Appl. Phys. Lett.*, vol. 88, no. 1, pp. 011114, Jan. 2006.

[23] G. Demetriou, J. P. Berube, R. Vallee, Y. Messaddeq, C. R. Petersen, D. Jain, O. Bang, C. Craig, D. W. Hewak, and A. K. Kar, "Refractive index and dispersion control of ultrafast laser inscribed waveguides in gallium lanthanum sulphide for near and mid-infrared applications," *Opt. Express*, vol. 24, no. 6, pp. 6350-6358, Mar. 2016.

[24] P. D. Townsend, P. J. Chandler, and L. Zhang, *Optical Effects of Ion Implantation*. Cambridge, UK: Cambridge Univ. Press, 1994.

[25] F. Chen, X. L. Wang, and K. M. Wang, "Development of ion-implanted optical waveguides in optical materials: A review," *Opt. Mater.*, vol. 29, no. 11, pp. 1523-1542, Jul. 2007.

[26] Y. Jiao and L. Wang, "Optical Channel Waveguide in KTiOAsO$_4$ Crystals Produced by O$^+$ ion Implantation," *J. Lightwave Technol.*, vol. 30, no. 10, pp. 1433-1436, May. 2012.

[27] M. F. Volk, S. Suntsov, C. E. Ruter, and D. Kip, "Low loss ridge waveguides in lithium niobate thin films by optical grade diamond blade dicing," *Opt. Express*, vol. 24, no. 2, pp. 1386-1391, Jan. 2016.

[28] K. Tanaka and T. Suhara, "Fabrication of 0.7 mu m(2) ridge waveguide in ion-sliced LiNbO$_3$ by proton-exchange accelerated chemical etching," *Jpn. J. Appl. Phys.*, vol. 54, no. 12, pp. 128002, Dec. 2015.

[29] F. Chen and J. Aldana, "Optical waveguides in crystalline dielectric materials produced by femtosecond laser micromachining," *Laser Photon. Rev.*, vol. 8, no. 2, pp. 251-275, Mar. 2014.

[30] C. Chen, R. Y. He, Y. Tan, B. Wang, S. Akhrnadaliev, S. Q. Zhou, J. R. V. de Aldana, L. L. Hu, and F. Chen, "Optical ridge waveguides in Er^{3+}/Yb^{3+} co-doped phosphate glass produced by ion irradiation combined with femtosecond laser ablation for guided-wave green and red upconversion emissions," *Opt. Mater.*, vol. 51, pp. 185-189, Jan. 2016.

[31] Y. Jia, F. Chen, J. R. Vazquez de Aldana, S. Akhmadaliev, and S. Zhou, "Femtosecond laser micromachining of Nd:GdCOB ridge waveguides for second harmonic generation," *Opt. Mater.*, vol. 34, no. 11, pp. 1913-1916, Sep. 2012.

[32] J. Martínez de Mendívil et al., "Mirrorless Yb^{3+}-Doped Monoclinic Double Tungstate Waveguide Laser Combining Liquid Phase Epitaxy and Multiplexed Beam fs Laser Writing," *J. Lightwave Technol.*, vol. 33, no. 23, pp. 4726-4730, Dec. 1 2015.

[33] J.F. Ziegler, Computer Code, SRIM. [Online] Available: http://www.srim.org.

[34] Rsoft Design Group, Computer software BeamPROP version 8.0. [Online] Available: http://www.rsoftdesign.com.

[35] D. Yevick and W. Bardyszewski, "Correspondence of variational finite-difference (relaxation) and imaginary-distance propagation methods for modal analysis," *Opt. Lett.*, vol. 17, no. 5, pp. 329-330, Mar. 1992.